

Conductance distribution across the Anderson transition in a random matrix model

Kazi A. Alam  and K. A. Muttalib 

Department of Physics, University of Florida, P.O. Box 118440, Gainesville, Florida 32611-8440, USA

 (Received 25 September 2022; revised 26 October 2022; accepted 27 October 2022; published 9 November 2022)

A model based on random matrix theory (RMT) is used to obtain the full conductance distribution $P(g)$ in three dimensions (3D) across the Anderson metal-insulator transition, and compared with the corresponding quasi-one-dimensional (Q1D) case where there is only a smooth crossover. We show that while the differences between the two are subtle, the details of the results from the RMT model agree very well with the existing numerical studies of the tight-binding Anderson model in 3D vs Q1D, including the critical region in 3D.

DOI: [10.1103/PhysRevB.106.184203](https://doi.org/10.1103/PhysRevB.106.184203)

I. INTRODUCTION

The Anderson transition in a disordered conductor is a quantum (zero temperature) phase transition from metal to insulator, as a function of the strength of disorder [1–3]. The scaling theory of localization [4] provides the framework that describes the transition in terms of the dimensionless conductance g , where $g \gg 1$ corresponds to a metal while $g \ll 1$ corresponds to an insulator, the transition happening at $g \sim 1$. However, absence of self-averaging leads to large mesoscopic fluctuations [5–10] and the mean or the typical values of g cannot adequately describe the transport properties of a disordered conductor, especially near the critical region where the variance of g becomes of the same order as the mean value [11–14]. In quasi-one-dimension (Q1D) where there is no phase transition, the shape of the distribution of conductance $P(g)$ changes from a Gaussian in the metallic limit to a log-normal in the insulating region, with a highly asymmetric “half log-normal” distribution in the crossover region [15–19]. Numerical results for the tight-binding Anderson model [20–22] as well as experiments on gated GaAs:Si wires [23] suggest that the distributions remain qualitatively similar in three dimensions (3D) across the transition, which suggests that it might be possible to consider $P(g)$ as an order-parameter function [24] for the Anderson transition.

Analytically, the distribution of conductance can in principle be reconstructed from the moments of the distribution if the moments are finite and unique. Within the field-theoretical framework, these moments have been calculated in a perturbation theory for small ϵ in $2 + \epsilon$ dimensions [25], but the distribution at the critical point obtained from the moments for $\epsilon = 1$ has a Gaussian head and power-law tails [26] which do not agree with numerical results in 3D. There is no field-theoretical framework where the conductance distribution can be obtained directly without first calculating the moments of the distribution.

In this work we propose to use a random matrix model (or log-gas model [27], to be precise) to study the full $P(g)$ as a function of disorder across the Anderson transition. It is a toy model that provides a possible analytical framework to study

a quantum phase transition in terms of an order-parameter function. Instead of trying to reconstruct the distribution from its moments, we obtain the full $P(g)$ directly from the joint probability distribution (JPD) $p_N(\{\lambda_i\})$ of the N transmission levels λ_i , $i = 1, 2, \dots, N$, where the conductance is a linear statistics given by [10,28]

$$g = \sum_i \frac{1}{1 + \lambda_i}. \quad (1.1)$$

In the large- N limit, the distribution of conductance then follows from

$$P(g) = \int_0^\infty \prod_{i=1}^N d\lambda_i p_N(\{\lambda_i\}) \delta\left(g - \sum_i \frac{1}{1 + \lambda_i}\right). \quad (1.2)$$

This method was used to obtain the highly asymmetric “half log-normal” distribution in the crossover region in Q1D mentioned above [15], based on the known JPD^{Q1D} for Q1D systems [29]. This has been shown to be equivalent in Q1D [30,31] to the nonlinear sigma-model description of the Anderson model [32,33].

The eigenvectors of the transmission matrices in Q1D are isotropically distributed at all disorder; therefore JPD^{Q1D} allows only a crossover from metallic to insulating regions. This isotropy assumption was built into the derivation of the Dorokhov-Mello-Pereyra-Kumar (DMPK) equation [34–37] whose solution gives the JPD^{Q1D} mentioned above. Clearly, the Anderson model in 3D requires a breaking of the isotropy symmetry, but the nature of the correlations of the eigenvectors of the corresponding transmission matrices in dimensions other than Q1D is highly nontrivial. By relaxing the isotropy assumption of the eigenvectors a generalized DMPK equation was obtained [38–41], which has been numerically solved [42] to show that the anisotropy correlations indeed include the effects of dimensionality in the full conductance distribution $P(g)$ and agree very well with numerically obtained $P(g)$ from the tight-binding Anderson model of disordered conductors. However, analytic solution of the generalized DMPK equation is not yet available except for the very strong disorder limit where only the smallest one or two transmission

eigenvalues play any significant role; in this limit a single anisotropy parameter has been shown to effectively contain the important effects of dimensionality [43–45].

Recently, a simplified generalized random matrix model with a single anisotropy parameter γ (a 3D generalization of the Muttalib-Borodin ensembles [46–48]) has been proposed and studied analytically [49,50]. The results, namely the exact density of the eigenvalues as a function of γ having a sharp crossover from metallic to insulating behavior, suggest that a model of JPD^{3D} inspired by the strong-disorder solution of the generalized DMPK equation might be used as a model to study in detail, within the random matrix theory (RMT) framework, the Anderson metal-insulator transition in terms of the full conductance distribution. In the present work we propose such a one-parameter RMT model and use the Monte Carlo method to evaluate the multidimensional integral in (1.2), thereby obtaining the full conductance distribution in both Q1D and 3D across the metal-insulator transition within the generalized RMT framework. While the Monte Carlo method has been previously used to obtain the full $P(g)$ in a Q1D system [51], a 3D system with a possible quantum phase transition has not been studied so far, due to the absence of an appropriate model. We show that the essential differences between Q1D and 3D in the conductance distribution is captured in remarkable detail by our simple one-parameter RMT model.

The rest of the paper is organized as follows. In Sec. II we introduce our model for JPD^{3D} based on the detailed numerical studies of the generalized DMPK equation. The model contains a single parameter γ which takes into account the correlations of the eigenvectors of the transmission matrices in 3D; $\gamma = 1$ reduces it to the Q1D limit JPD^{Q1D}. This allows us to compare 3D vs Q1D within the same framework in great detail. We briefly describe our method based on Monte Carlo in Sec. III. In Sec. IV we present our results which show that the major differences in $P(g)$ between Q1D and 3D around the critical region lie in the range $g \gtrsim 1$. These differences agree very well with numerical results from the tight-binding Anderson model [20]. In other words, our model of JPD^{3D} captures the essential features of dimensionality via the single parameter γ . Section V contains our summary and conclusion.

II. THE MODEL

The standard model to study the metal-insulator transition is the Anderson model on a d -dimensional lattice, defined by the Hamiltonian

$$H = W \sum_i \epsilon_i c_i^\dagger c_i + \sum_{\langle i,j \rangle} c_i^\dagger c_j, \quad (2.1)$$

where c_i^\dagger and c_i are the creation and annihilation operators for electrons. Here ϵ_i is the energy of site i , randomly distributed with (typically) a box distribution $|\epsilon_i| \leq 1/2$, W is the strength of disorder, and $\langle i, j \rangle$ refers to the sum over nearest-neighbor sites; the hopping strength is taken to be 1. The model has been extensively investigated numerically, including the full distribution $P(g)$ across the transition [22], which occurs at a critical disorder W_c in 3D. However, as mentioned above, currently available theoretical techniques are not adequate to study $P(g)$ from (2.1) analytically.

Instead of starting from a Hamiltonian, an alternative way to study the conductance distribution is to start directly with a transfer matrix formulation. A disordered three-dimensional conductor of length L_z and cross section L^2 connected to two ideal leads has N transmission channels, with $N \propto L^2$. Transport properties are then determined by the $2N \times 2N$ transfer matrix M connecting the outgoing flux to the incoming flux across L_z . Flux conservation leads to a general form for M given by [10,35]

$$M = \begin{pmatrix} v_1 & 0 \\ 0 & v_3 \end{pmatrix} \begin{pmatrix} \sqrt{1+\lambda} & \sqrt{\lambda} \\ \sqrt{\lambda} & \sqrt{1+\lambda} \end{pmatrix} \begin{pmatrix} v_2 & 0 \\ 0 & v_4 \end{pmatrix}. \quad (2.2)$$

Here v_i are $N \times N$ unitary matrices, and λ is a diagonal matrix with non-negative elements. The $N \times N$ transmission matrix tt^\dagger can be written as $tt^\dagger = v_4(1+\lambda)^{-1}v_4^\dagger$ and diagonalizing tt^\dagger gives the eigenvalues λ as well as the elements of the matrix v . If the JPD $p_N(\{\lambda_i\})$ of the eigenvalues are known in the large- N limit, then the full distribution of conductance is given by (1.2). In Q1D, which assumes isotropy of the eigenvectors in v , $p_N^{\text{Q1D}}(\{\lambda_i\})$ is known analytically [29]. While the exact solution as a determinant is complicated, a good description in the region with $g \gg 1$ is given by

$$\begin{aligned} \text{JPD}^{\text{Q1D}} &\equiv p_N^{\text{Q1D}}(\{x_i\}) \\ &\propto \prod_{i<j} |x_i^2 - x_j^2|^{\frac{\beta}{2}} |\sinh^2 x_i - \sinh^2 x_j|^{\frac{\beta}{2}} \prod_{i=1}^N e^{-V(x_i)}, \\ V(x_i) &= \frac{\Gamma}{2} x_i^2 - \frac{1}{2} \ln(x_i \sinh 2x_i); \quad \sinh^2 x_i = \lambda_i, \end{aligned} \quad (2.3)$$

where Γ is a parameter that determines the average conductance. Here $\beta = 1, 2, 4$ correspond to the orthogonal, unitary, and symplectic symmetry classes, respectively [52]. Compared to the standard Wigner-Dyson random matrix model [52,53] originally proposed to describe nuclear energy level correlations,

$$p_N^{\text{WD}}(\{x_i\}) \propto \prod_{i<j} |x_i - x_j|^\beta \times \prod_{i=1}^N e^{-\Gamma x_i^2}, \quad (2.4)$$

the two-particle interaction $|\sinh^2 x_i - \sinh^2 x_j|$ as well as the logarithmic terms in the single-particle confining potential $V(x)$ in (2.3) arise from the solution of the DMPK equation [29,54] that describes the evolution of the JPD with length in a Q1D disordered conductor. JPD^{Q1D} in (2.3) was used in [15–17] for $\beta = 2$ to obtain the Gaussian, log-normal, and “half log-normal” distributions in the metallic, insulating, and the crossover region (between metal and insulator), respectively, using Eq. (1.2).

We propose that the model for the one-parameter generalization to 3D in the region around the transition has the form inspired by the solution of the generalized DMPK equation in the insulating limit [43–45]

$$\begin{aligned} \text{JPD}^{\text{3D}} &\equiv p_N^{\text{3D}}(\{x_i\}) \\ &\propto \prod_{i<j} |x_i^2 - x_j^2|^{\frac{\beta}{2}\gamma} |\sinh^2 x_i - \sinh^2 x_j|^{\frac{\beta}{2}\gamma} \prod_{i=1}^N e^{-V(x_i)}, \\ &0 < \gamma < 1. \end{aligned} \quad (2.5)$$

For simplicity, the confining potential $V(x)$ has been kept the same as in (2.3). The phenomenological parameter γ appearing as exponents of the interaction terms is an approximation of the matrix γ_{ab} related to the eigenvector correlations of the matrix v in (2.2) given by [39]

$$K_{ab} \equiv \sum_i \langle |v_{ia}|^2 |v_{ib}|^2 \rangle; \quad \gamma_{ab} = \frac{2K_{ab}}{K_{aa}}, \quad \gamma \approx \gamma_{12}, \quad (2.6)$$

where the angular bracket $\langle \cdot \rangle$ indicates an average over the realizations of disorder. Apparently at very strong disorder the exponent is important for the second interaction term only, and it has been shown numerically to contain information about the strength of disorder as well as the dimensionality of the system [43–45]. We find that including the exponent on both interaction terms [55] as in (2.5) allows us to go beyond the very strong disorder limit, such that the region close to both sides of the critical disorder can be explored.

Isotropy of the eigenvectors would imply

$$K_{ab}^{\text{Q1D}} = \frac{1 + \delta_{ab}}{N + 1}; \quad \Rightarrow \gamma = 1. \quad (2.7)$$

Thus JPD^{3D} given by (2.5) reduces to JPD^{Q1D} in (2.3) when $\gamma = 1$. For any $\gamma < 1$, the eigenvectors are no longer isotropic. While a single anisotropy parameter may not contain all effects of dimensionality as well as strength of disorder, it does allow us to study the important differences in any linear statistics of the eigenvalues, like the conductance (1.1), in Q1D vs 3D, within the same level of accuracy. Note that γ is also presumably scale dependent, becoming scale invariant at the critical point [44]. However in this toy model we consider γ as an independent phenomenological parameter related to the disorder of the system, which is characterized by the average conductance $g_0 = \langle g \rangle$. Our small- N studies will not allow us to identify the critical point γ_c or the corresponding g_c by, e.g., considering the scale invariance of the distribution. Nevertheless, once the critical point is identified by other means, changing γ allows us to study the changes in the shape of the distribution across the Anderson metal-insulator transition. Thus, the model provides a framework where $P(g)$ can be used as an order-parameter function that describes a quantum phase transition.

The parameter Γ in Q1D determines the average conductance. In 3D, both Γ and the anisotropy parameter γ are related to the strength of disorder. Numerical studies suggest a monotonic relationship between the two [44], so there is again only a single parameter that characterizes our model. The relationship $\Gamma(\gamma)$ must satisfy certain known limits, namely, $\Gamma \gg 1$ when $\gamma \rightarrow 1$ and $\Gamma \ll 1$ when $\gamma \rightarrow 0$. Numerically it has been established that $\Gamma \sim 2\gamma$ near the critical point of the Anderson transition. We thus take the simplest relationship that satisfies all three known limits, $\Gamma = c\gamma/(1 - \gamma)$. Here the constant c is of order 1 and fixes the average conductance $g_0 = \langle g \rangle$ for a given value of γ . We find that for $N = 6$, $c = 1.7$ gives values of g_0 around the transition that are close to the values of g_0 obtained from the numerical solutions of the Anderson model and gives best fit for the 3D critical conductance. Note that once $c = 1.7$ is fixed, disorder in 3D is entirely characterized by the remaining single parameter γ of the model.

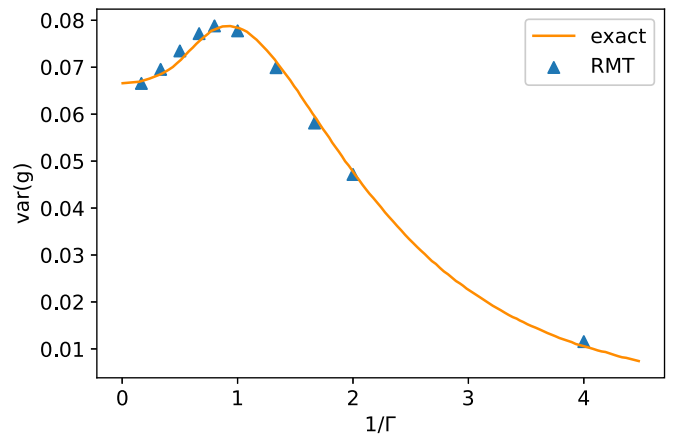


FIG. 1. Variance for Q1D, $\beta = 2$. Exact variances (solid line) are from nonlinear σ model, taken from [17]. RMT results for $N = 6$ are from our MCMC computation.

III. METHOD

We use the Markov chain Monte Carlo (MCMC) method to evaluate the multidimensional integral (1.2). MCMC is a good choice for our purpose for many different reasons. Numerical integrals get very slow beyond dimension 3. Monte Carlo is the default choice for any such integral in higher dimensions. Particularly for a JPD like (2.5), we cannot employ other methods (e.g., orthogonal polynomials) for RMT computations due to the exponent γ . MCMC also allows us to evaluate $P(g)$, g_0 , $\text{var}(g)$, etc., in a straightforward way. We will choose $N = 6$, as was chosen in the Monte Carlo studies of [51] for Q1D. To make sure that our procedure works we reproduced the variance curve for Q1D [17] for $\beta = 2$ in Fig. 1. It is clear from the figure that $N = 6$ gives very good results for all disorder in Q1D. In particular, it reproduces the well-known result $\text{var}(g) = 2/(15\beta)$ in the weakly disordered region. We have checked that the obtained variances at all disorder converge toward the exact values as N is increased. In 3D, on the other hand, such small values of N give a variance in the weakly disordered region which is smaller than the known result. The agreement improves as N is increased, and we find that one needs $N \gg 6$ to achieve the correct result. This is because in the weakly disordered region a large number of channels [characterized by a large number of small eigenvalues λ_i ; see (1.1)] contribute to the conductance. Since our resources restrict us to a choice of $N = 6$, this implies that we will be restricted to stronger disorder, where only a small number of channels (with relatively larger eigenvalues) contribute. We find that with our model (2.5), this includes the critical region around the metal-insulator transition which is our main focus in this study. Clearly, in order to identify the critical point and to explore the critical region further beyond the scope of the current focus, a systematic study of the N dependence of $P(g)$ for much larger N would be essential.

We emphasize that the critical conductance is not a universal quantity, and we do not try to match the values of the conductance between the RMT and the tight-binding Anderson model by, e.g., fine-tuning the phenomenological relationship $\Gamma(\gamma)$ as mentioned in Sec. II. Thus for a given disorder our values of g_0 from RMT will not in general agree

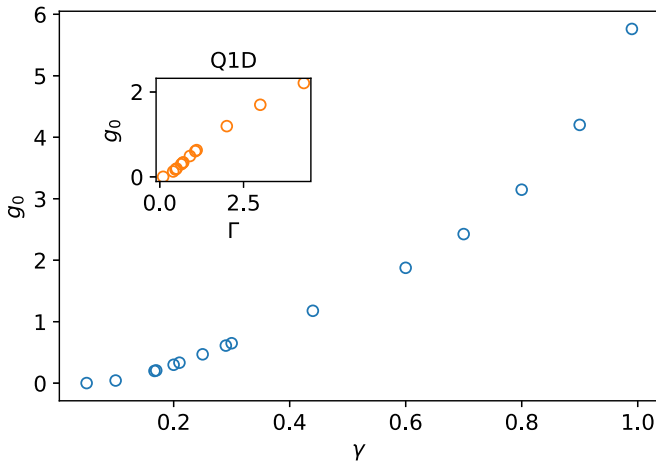


FIG. 2. Average conductance $g_0 = \langle g \rangle$ vs γ in 3D for $N = 6$. Inset shows g_0 vs Γ in Q1D.

with the values obtained numerically in [20] from the Anderson model (2.1). Nevertheless, we can compare the $P(g)$ between the RMT and the Anderson model unambiguously if we always characterize the disorder by the average conductance g_0 . We achieve this in the following way: In [20], for the Anderson model, $P(g)$ in Q1D and 3D were compared where both had the same average conductance, say g_0^A . Within the RMT model we do the same, for an average conductance g_0 that may not be equal to g_0^A . For a fixed N , we first find a value of the Q1D parameter Γ for which our full $P(g)$ best matches with the full numerical $P(g)$ of the Anderson model, especially near the tail of the distribution $g \gtrsim 1$. (The high sensitivity of the distribution to the choice of Γ allows us, within our accuracy, to choose the “best match” simply by eye estimation.) This Γ then fixes the value of g_0 in Q1D (see inset of Fig. 2), which may not agree with the g_0^A of the Anderson model. We then find a 3D system in our model with the same g_0 , characterized by the 3D parameter γ (see Fig. 2), which then determines the full $P(g)$ in 3D. Thus the Q1D and 3D distributions within the RMT model can be compared with the corresponding distributions of the Anderson model directly, without having to match the average conductance between the two very different models.

IV. RESULTS

In numerical evaluations of the tight-binding Anderson model, the strength of disorder is specified by, e.g., the width of the random distribution of the site energies W . In the generalized RMT framework discussed above, Γ in Q1D and γ in 3D are phenomenological parameters that depend on disorder. To compare the results, it is more appropriate to choose the average conductance $g_0 \equiv \langle g \rangle$ as the measure of the strength of disorder. Figure 2 shows how g_0 changes with γ in 3D and Γ in Q1D for $N = 6$.

We primarily consider the orthogonal case of $\beta = 1$ in detail because Markoš [20] has done an extensive numerical comparison of the 3D vs Q1D conductance distributions in the tight-binding Anderson model (2.1) which can be compared with our 3D vs Q1D RMT models. The $\beta = 2$ case, where

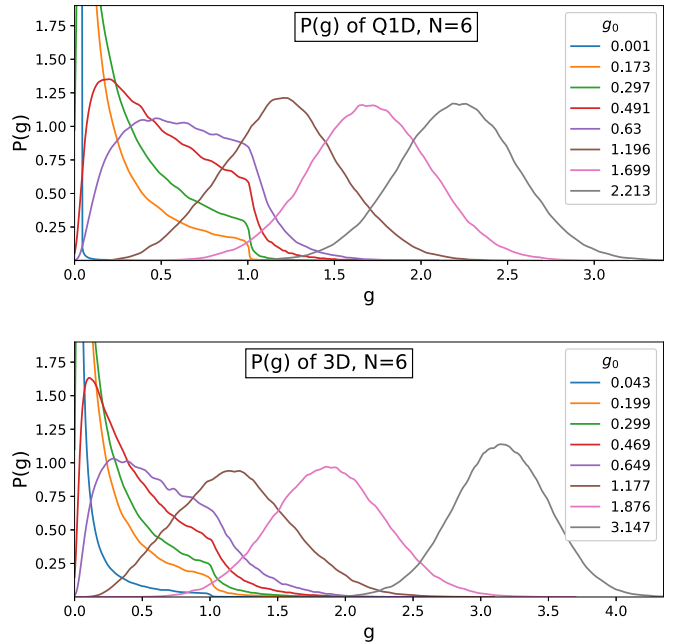


FIG. 3. $P(g)$ for different values of g_0 , showing the change in the shape of the distribution from metallic ($g_0 \gg 1$) to insulating regions ($g_0 \ll 1$). Top panel is for Q1D, while the bottom panel, showing very similar changes, is for 3D.

only limited numerical results are available, will be considered briefly toward the end.

Figure 3 shows $P(g)$ for different values of disorder characterized by the average conductance g_0 , for 3D as well as Q1D. The distribution changes from a Gaussian in the metallic region ($g_0 \gg 1$) to a very wide and highly asymmetric distribution in the insulating region ($g_0 \ll 1$), with broad unusual shapes in the intermediate regions for both 3D and Q1D. While the changes in the shape of the distribution for either 3D or Q1D are quite dramatic, differences between Q1D and 3D are not obvious. In the following, we discuss the similarities and the differences between Q1D and 3D distributions, comparing them with numerical results whenever available. Note that while we do not obtain the critical point for 3D independently in our work, it is possible to identify it by comparing with the existing numerical results, as we show later.

It is well known for Q1D systems (and $\beta = 1$) that in the weakly disordered region the conductance distribution is a Gaussian [16], with a universal variance $\frac{2}{15} \approx 0.13$ [54]; the distribution remains Gaussian in 3D, with a variance ≈ 0.3 [56]. Figure 4 shows $P(g)$ in the weakly disordered regions for both Q1D and 3D for similar average conductances in the RMT model, compared with the numerical solutions [20] of the tight-binding Anderson model (2.1). While this phenomenon of a limiting Gaussian distribution applies to some general RMT (or log-gas) ensembles [57–59], to the best of our knowledge it has not been proven for a more general JPD like (2.5). Our result suggests that this should be true also for a log-gas model like (2.5), possibly with a more general single-particle potential.

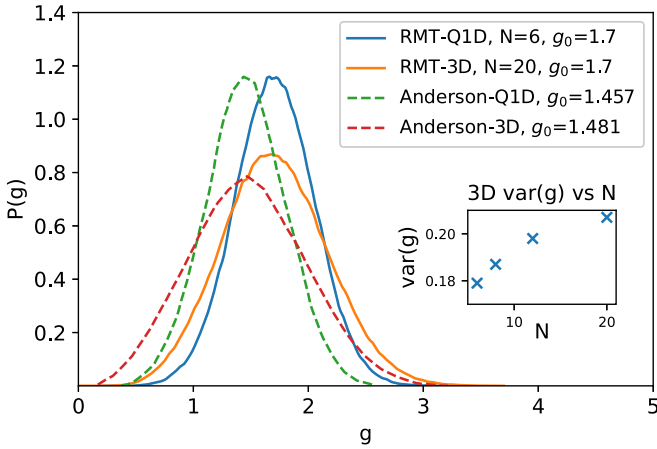


FIG. 4. $P(g)$ in the weakly disordered region from our RMT model compared with numerical results from the Anderson model obtained in [20]. For both 3D and Q1D, $P(g)$ are Gaussian. The variance in Q1D is 0.13, for both RMT and the Anderson model. In 3D, the variance for the Anderson model is 0.27, while it is 0.21 for RMT for $N = 20$. The inset suggests that the RMT variance tends towards the numerical results as N increases.

The differences between Q1D and 3D in Fig. 4 are very similar between the RMT vs Anderson models. However, while the Q1D variance is given correctly for $N = 6$ in the RMT model, it requires $N > 20$ to give the correct 3D variance. As N is increased from $N = 6$, the variance increases from 0.18 toward the value of the Anderson model. As mentioned in Sec. III, this implies that although $N = 6$ gives qualitatively good results even in the weakly disordered region, it is too small for quantitative comparison at weak disorder because many channels contribute to the conductance in this region. Since we are limited to $N = 6$, we keep our focus on stronger disorder, where only a few channels contribute and our results are more reliable.

To focus on the differences between Q1D and 3D in the strongly disordered region, we evaluate the integral

$$I_1 = \int_1^\infty P(g) dg \quad (4.1)$$

as suggested in [20]. Figure 5 shows the results as a function of g_0 for both 3D and Q1D. The differences, increasing with decreasing g_0 , are in excellent agreement with numerical results. Thus the RMT model, with the exponent γ of the two-level interaction terms in (2.5), captures the important 3D features that distinguish $P^{3D}(g)$ from the corresponding Q1D distribution $P^{Q1D}(g)$.

To explore the differences between 3D vs Q1D further, we therefore focus on the tails near $g \gtrsim 1$ and compare the distributions for two different values of disorder in detail in Fig. 6, one on the metallic side and one on the insulating side of the critical region. The results from our RMT model confirm the numerical results of [20] that the Q1D tail for a given g_0 at $g \gtrsim 1$ is much sharper than the corresponding 3D tail for the same g_0 . The distribution for $g < 1$ is very similar between 3D and Q1D, which also agrees with the numerical results. Note that there is a discontinuity in the slope at $g = 1$ for $g_0 \ll 1$ in the RMT model in Q1D as shown analytically

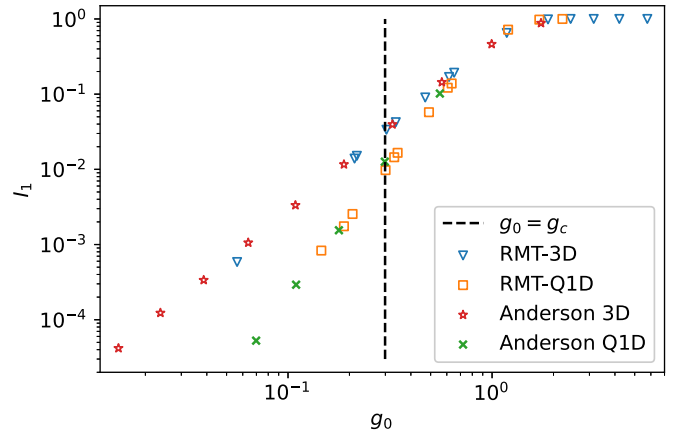


FIG. 5. $I_1 \equiv \int_1^\infty P(g) dg$ for different g_0 for 3D vs Q1D from the RMT model, compared with numerical results of the Anderson model [20].

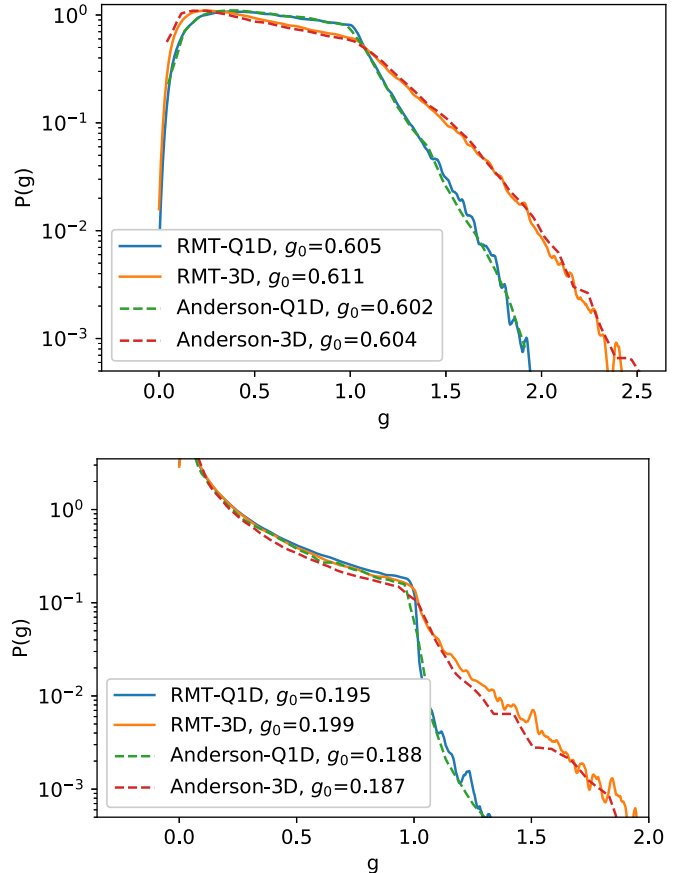


FIG. 6. Detailed comparison of the tails of the distribution for 3D and Q1D cases obtained from (1.2) for the RMT model compared to the numerical solutions of the Anderson model [20]. To keep the comparisons meaningful, both Q1D and 3D distributions are chosen to have the same g_0 within each model. Top panel corresponds to a region on the metallic side, while the bottom panel corresponds to the insulating side of the critical region. In both cases, Q1D tails drop much faster than the 3D tails, the most distinguishing difference between Q1D and 3D distributions.

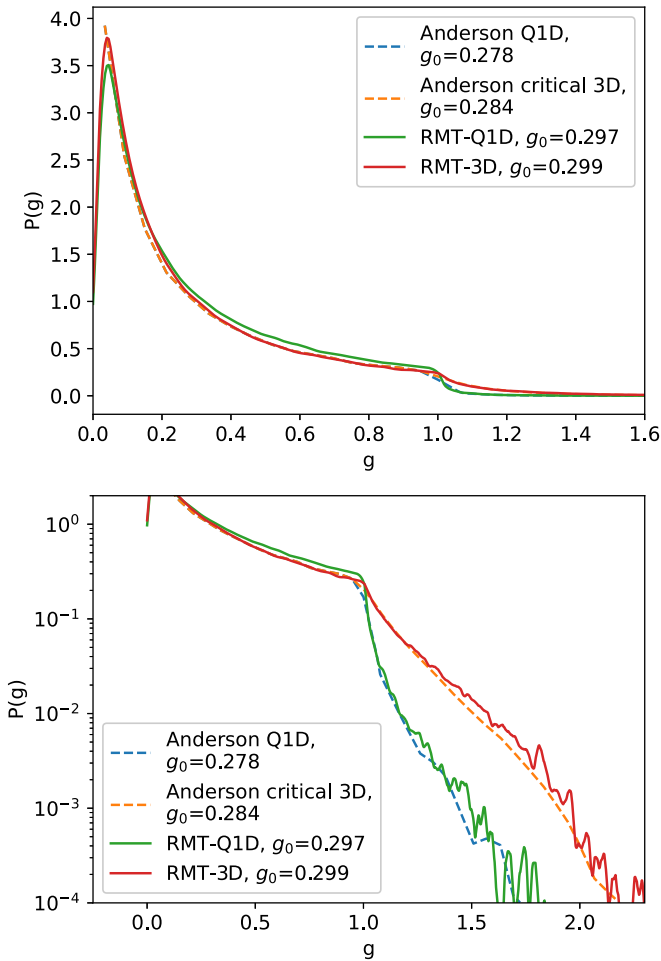


FIG. 7. Critical distribution for 3D, compared with numerical results of the Anderson model from [20]. Also shown are the Q1D results with similar values of g_0 within each model. While the bottom panel is on a logarithmic scale emphasizing the differences in the tails $g > 1$ of the distributions between Q1D and 3D, the top panel in linear scale shows that the overall agreement with the Anderson model remains good for $g < 1$ as well.

in [19] which agrees with the numerical results in [21]; our results are consistent with it.

Given that the model gives $P(g)$ very well on both sides of the transition, ideally we should be able to identify the critical point from finite-size scaling; the distributions should become scale invariant at the critical point. Unfortunately, since we work with a small fixed value of N and do not know how the phenomenological single-particle potential parameter $\Gamma(\gamma)$ depends on N , we cannot identify the critical point. Nevertheless, we can compare and match the numerically known critical distribution $P_c(g)$ by exploring the range of distributions in the critical region, between the metallic and insulating distributions of Fig. 6, and comparing with the $P_c(g)$ from numerical studies of the Anderson model. Figure 7 shows $P(g)$ that matches with numerical $P_c(g)$ from [20]. The tail agrees very well, and the difference with the corresponding Q1D for a similar value of g_0 also agrees with numerical results. We also show the $g < 1$ region in linear scale to show the overall agreement.

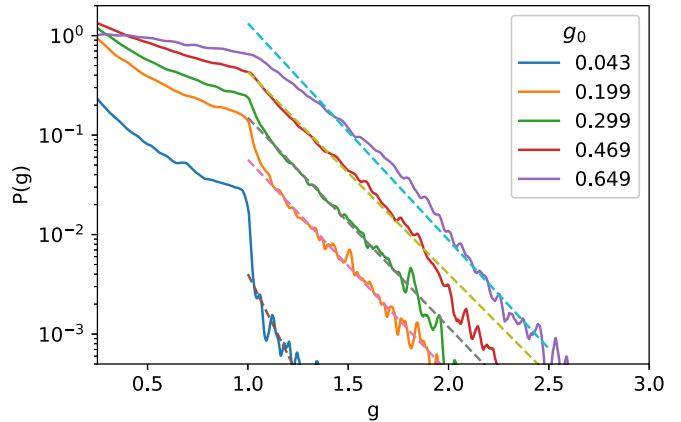


FIG. 8. Tails of the distribution to show the change in the curvature across the critical region. Green plot corresponding to the critical conductance at $g_c = 0.299$ is consistent with zero curvature, implying an exponential tail in linear scale. Tails for $g_0 > g_c$ have increasing slopes, while those for $g_0 < g_c$ are consistent with zero curvature.

As a measure of systematic change, we show in Fig. 8 a comparison of how the tails of the distribution change across the transition. In the range $g > 1$, the metallic side has a clear curvature with a slope increasing with g , while the critical point with $g_0 = 0.299$ (see Fig. 7) is consistent with a zero curvature. Other plots on the insulating side are also consistent with zero curvature. Note that the y axis is logarithmic, so a straight line implies an exponential decay. While the metallic side near the critical point is not yet Gaussian, it matches with Gaussian at weaker disorder. Thus the tails of the distribution change from a Gaussian in the metallic region (see Fig. 4) to an exponential at the critical point and beyond. The existence of a curvature (a metal), or no curvature (the insulator), could then be an order parameter that distinguishes between the two phases. However, our computations at $N = 6$ with large fluctuations for $P(g) < 10^{-3}$ restrict our ability to explore the possibilities any further.

Finally, we briefly discuss the unitary case. Although detailed numerical studies for $P(g)$ in the unitary case are not available, we compare in Fig. 9 the critical distribution for $\beta = 2$ and $\beta = 1$ obtained in [11] with our RMT model. Note that a factor of 2 for spin has been included as in the numerical evaluation so that the tail occurs at $g = 2$ instead of $g = 1$. However, the numerical results do not focus on the tails, and we just show the overall difference between $\beta = 2$ and $\beta = 1$; the agreement shows that the RMT model correctly describes the unitary symmetry class as well.

V. SUMMARY AND DISCUSSION

The Wigner-Dyson random matrix theory was invented to explain the universal spectral properties of energy levels of heavy nuclei. It has been shown since then that the Wigner-Dyson RMT describes a wide variety of ergodic systems like quantum dots that are essentially zero-dimensional [53]. The solution of the DMPK equation showed that RMT can describe a Q1D system provided it contains an additional two-particle interaction term [29]. However, disorder in a

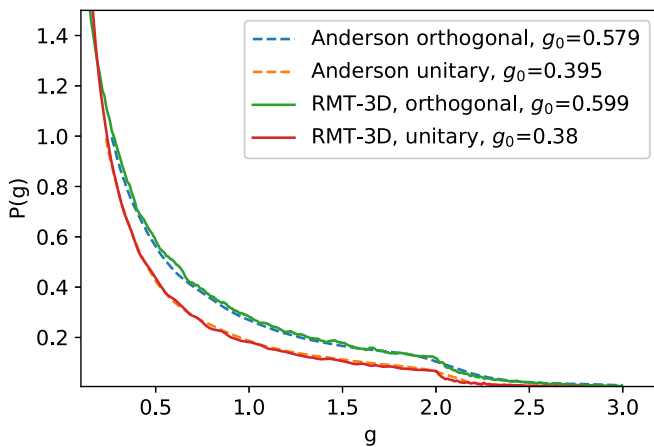


FIG. 9. $P(g)$ for the unitary case $\beta = 2$ in Eq. (2.5), compared with numerical results of [11]. A factor of 2 for spin has been included in the numerical evaluation so that the tail occurs at $g = 2$ instead of $g = 1$; the RMT computation has been modified accordingly.

Q1D RMT model is different from 3D. Starting with weak disorder, the effective disorder in a Q1D system increases with increasing length (in the direction of the current) so that the system always becomes insulating in the limit of large length, even with weak disorder. Therefore the Q1D insulating region in (2.3) is very different from the Anderson insulators in 3D and the JPD^{Q1D} does not have a metal-insulator transition.

A true insulating region in an RMT model, and as a consequence a metal-insulator transition, requires breaking the isotropy of the transmission eigenvectors. Roughly speaking, an isotropic eigenvector of an N -channel transmission matrix, corresponding to a good metal with all channels “open,” would have all its components equal in magnitude, $\sim 1/\sqrt{N}$. An eigenvector of an insulator, on the other hand, would have only a few ($n \ll N$) open channels with components $\sim 1/\sqrt{n}$, the remaining channels being closed, breaking the isotropy symmetry. Thus away from the critical region, the parameter γ in (2.6) can be crudely interpreted as the fraction n/N of channels that are effectively open. In contrast in Q1D, an insulator is obtained by keeping the isotropy of the eigenvectors (at weak disorder) but decreasing Γ (associated with increasing length) in the single-particle potential sufficiently, thus allowing all eigenvalues to become very large, leading to $g_0 \ll 1$. In the current work we show that the exponent

$0 < \gamma < 1$ in our model (2.5) indeed allows for a dimensionality dependence in $P(g)$. The differences in $P(g)$ between the Q1D vs 3D around the critical region are primarily in the tails of the distribution near $g \gtrsim 1$ and the results of our model are in excellent agreement with numerical results from the tight-binding Anderson model. In particular, the tail of the critical distribution in 3D agrees very well with numerical results after the critical point is identified. This suggests that (2.5) can be used as an analytically tractable model to study the Anderson metal-insulator transition in terms of the full $P(g)$. Since numerical evaluations of $P(g)$ directly from the generalized DMPK equation also show excellent agreement with the tight-binding Anderson model [42], our results suggest that model (2.5) might be a reasonable solution of the generalized DMPK equation [38,39] for all disorder.

We note that a rotationally invariant *critical* random matrix model for the energy levels has been proposed which has the original Wigner-Dyson interaction form but a soft single-particle potential which grows only as the square of a logarithm at large distances [60]; the spacing distribution from this model agrees very well with the critical spacing distribution obtained from tight-binding Anderson model [61]. A solvable random matrix model has been used to obtain conductance distributions within such a rotationally invariant transmission matrix model [62,63]. It has been argued that such models have spontaneous symmetry breaking in order to be critical [64]. In contrast, the parameter γ in our current model for transmission levels explicitly breaks the isotropy symmetry of the transmission eigenvectors.

Our calculations are done with a small fixed N and the model contains only a scale-independent phenomenological single-particle potential. These limitations prevent us from obtaining the exact critical point from the scaling properties of $P(g)$. A systematic study with larger values of N is needed to identify the critical point independently and further explore the critical region within the RMT framework. One interesting possibility is to explore Fig. 8 further, if the critical distribution can be identified from the curvature of the tails near $g \gtrsim 1$.

ACKNOWLEDGMENTS

We are grateful to P. Markoš and P. Wölfle for critical reading of the manuscript and valuable comments and suggestions.

[1] P. W. Anderson, *Phys. Rev.* **109**, 1492 (1958).
 [2] P. A. Lee and T. V. Ramakrishnan, *Rev. Mod. Phys.* **57**, 287 (1985).
 [3] F. Evers and A. D. Mirlin, *Rev. Mod. Phys.* **80**, 1355 (2008).
 [4] E. Abrahams, P. W. Anderson, D. C. Licciardello, and T. V. Ramakrishnan, *Phys. Rev. Lett.* **42**, 673 (1979).
 [5] A. D. Stone, *Phys. Rev. Lett.* **54**, 2692 (1985).
 [6] P. A. Lee and A. D. Stone, *Phys. Rev. Lett.* **55**, 1622 (1985).
 [7] B. L. Altshuler, *Sov. Phys. JETP* **64**, 127 (1985).
 [8] S. Washburn and R. A. Webb, *Adv. Phys.* **35**, 375 (1986).
 [9] Y. Imry, *Europhys. Lett.* **1**, 249 (1986).

[10] A. D. Stone, P. Mello, K. A. Muttalib, and J.-L. Pichard, in *Mesoscopic Phenomena in Solids*, edited by B. L. Altshuler, P. A. Lee, and R. A. Webb (North-Holland, 1991), p. 369.
 [11] K. Slevin and T. Ohtsuki, *Phys. Rev. Lett.* **78**, 4083 (1997).
 [12] P. Markoš and B. Kramer, *Philos. Mag. B* **68**, 357 (1993).
 [13] P. Markos, *Europhys. Lett.* **26**, 431 (1994).
 [14] A. M. Somoza, J. Prior, and M. Ortuno, *Phys. Rev. B* **73**, 184201 (2006).
 [15] K. A. Muttalib and P. Wölfle, *Phys. Rev. Lett.* **83**, 3013 (1999).
 [16] P. Woelfle and K. A. Muttalib, *Ann. Phys. (Leipzig)* **8**, 753 (1999).

- [17] V. A. Gopar, K. A. Muttalib, and P. Wolfle, *Phys. Rev. B* **66**, 174204 (2002).
- [18] A. García-Martín and J. J. Saenz, *Phys. Rev. Lett.* **87**, 116603 (2001).
- [19] K. A. Muttalib, P. Woelfle, A. Garcia-Martin, and V. A. Gopar, *Europhys. Lett.* **61**, 95 (2003).
- [20] Peter Markoš, *Phys. Rev. B* **65**, 104207 (2002).
- [21] P. Markos, in *Anderson Localization and Its Ramifications*, Lecture Notes in Physics, edited by T. Brandes and S. Kettmann (Springer, Berlin, 2003), Vol. 630, pp. 53–64.
- [22] M. Rühländer, P. Markos, and C. M. Soukoulis, *Phys. Rev. B* **64**, 212202 (2001).
- [23] W. Poirier, D. Mailly, and M. Sanquer, *Phys. Rev. B* **59**, 10856 (1999).
- [24] For an example of an order-parameter function, see G. Parisi, *Phys. Rev. Lett.* **43**, 1754 (1979).
- [25] B. L. Altshuler, V. E. Kravtsov, and I. V. Lerner, *Sov. Phys. JETP* **64**, 1352 (1986).
- [26] B. Shapiro, *Phys. Rev. Lett.* **65**, 1510 (1990).
- [27] P. J. Forrester, *Log-Gases and Random Matrices* (Princeton University Press, 2010).
- [28] K. A. Muttalib, J.-L. Pichard, and A. D. Stone, *Phys. Rev. Lett.* **59**, 2475 (1987).
- [29] C. W. J. Beenakker, *Rev. Mod. Phys.* **69**, 731 (1997).
- [30] P. W. Brouwer and K. Frahm, *Phys. Rev. B* **53**, 1490 (1996).
- [31] B. Rajaei, *Phys. Rev. B* **53**, R13235 (1996).
- [32] K. Efetov and A. Larkin, *Sov. Phys. JETP* **58**, 444 (1983).
- [33] A. D. Mirlin, A. Muller-Groeling, and M. R. Zirnbauer, *Ann. Phys. (NY)* **236**, 325 (1994).
- [34] O. N. Dorokhov, *JETP Lett.* **36**, 318 (1982).
- [35] P. A. Mello, P. Pereyra, and N. Kumar, *Ann. Phys. (NY)* **181**, 290 (1988).
- [36] G. Mil'nikov and N. Mori, *Phys. Rev. B* **88**, 155406 (2013).
- [37] See, however, M. Capello and M. Caselle, *J. Phys.: Condens. Matter* **15**, 6845 (2003), for clustered solutions of DMPK that break the isotropy symmetry.
- [38] K. A. Muttalib and J. R. Klauder, *Phys. Rev. Lett.* **82**, 4272 (1999).
- [39] K. A. Muttalib and V. A. Gopar, *Phys. Rev. B* **66**, 115318 (2002).
- [40] A. Douglas and K. A. Muttalib, *Phys. Rev. B* **80**, 161102(R) (2009).
- [41] A. Douglas and K. A. Muttalib, *Phys. Rev. B* **82**, 035121 (2010).
- [42] J. Brndiar, R. Derian, and P. Markos, *Phys. Rev. B* **76**, 155320 (2007).
- [43] P. Markoš, K. A. Muttalib, P. Wölfle, and J. R. Klauder, *Europhys. Lett.* **68**, 867 (2004).
- [44] K. A. Muttalib, P. Markos, and P. Wölfle, *Phys. Rev. B* **72**, 125317 (2005).
- [45] A. Douglas, P. Markos, and K. A. Muttalib, *J. Phys. A: Math. Theor.* **47**, 125103 (2014).
- [46] K. A. Muttalib, *J. Phys. A: Math. Gen.* **28**, L159 (1995).
- [47] A. Borodin, *Nucl. Phys. B* **536**, 704 (1998).
- [48] D. Wang and L. Zhang, *J. Funct. Anal.* **282**, 109380 (2022).
- [49] S. Yadav, K. Alam, K. A. Muttalib, and D. Wang, *J. Phys. A: Math. Theor.* **53**, 015001 (2020).
- [50] S. Yadav, K. Alam, K. A. Muttalib, and D. Wang, *Phys. Rev. E* **103**, 042137 (2021).
- [51] L. S. Froufe-Perez, P. Garcia-Mochales, P. A. Serena, P. A. Mello, and J. J. Saenz, *Phys. Rev. Lett.* **89**, 246403 (2002).
- [52] M. L. Mehta, *Random Matrices*, 2nd ed. (Academic, 1991).
- [53] T. Guhr, A. Mueller-Groeling, and H. Weidenmueller, *Phys. Rep.* **299**, 189 (1998).
- [54] C. W. J. Beenakker and B. Rajaei, *Phys. Rev. B* **49**, 7499 (1994).
- [55] This can be thought of as a generalized beta ensemble; see, e.g., I. Dumitriu and A. Edelman, *J. Math. Phys.* **43**, 5830 (2002); T. Baker and P. Forrester, *Commun. Math. Phys.* **188**, 175 (1997).
- [56] P. A. Lee, A. D. Stone, and H. Fukuyama, *Phys. Rev. B* **35**, 1039 (1987).
- [57] L. Pastur, *J. Math. Phys.* **47**, 103303 (2006).
- [58] J. Breuer and M. Duits, *J. Amer. Math. Soc.* **30**, 27 (2017).
- [59] I. Dumitriu and E. Paquette, *Random Matrices: Theory Appl.* **01**, 1250013 (2012).
- [60] K. A. Muttalib, Y. Chen, M. E. H. Ismail, and V. N. Nicopoulos, *Phys. Rev. Lett.* **71**, 471 (1993).
- [61] S. M. Nishigaki, *Phys. Rev. E* **59**, 2853 (1999).
- [62] Y. Chen, M. E. H. Ismail, and K. A. Muttalib, *J. Phys.: Condens. Matter* **4**, L417 (1992).
- [63] Y. Chen, M. E. H. Ismail, and K. A. Muttalib, *J. Phys.: Condens. Matter* **5**, 177 (1993).
- [64] V. E. Kravtsov and K. A. Muttalib, *Phys. Rev. Lett.* **79**, 1913 (1997).